Near-field optical and atomic force constraints for super-resolution 3D deconvolution in far-field optical microscopy

Noel Axelrod[a,b], Anna Radko[a,b], Nissim Ben-Yosef[a], Artium Khatchatouriants[a,b], Millet Treinin[c], and Aaron Lewis [a,b]*

Division of Applied Physics [a], Department of Ophthalmology Hadassah Laser Center [b] and Department of Physiology [c], The Hebrew University of Jerusalem, Israel, IL-91904

ABSTRACT

We demonstrate that near-field optical and atomic force microscopy data can be used for super-resolution three-dimensional (3-D) image restoration in optical sectioning fluorescence microscopy. A crucial feature in this approach is the full integration of such data sets with digital far-field images. The scanned probe data is used to provide modalities for boundary constraints which define surface optical information and spatial domains of optical alterations in a sample with a spatial precision that has been unachievable in the past. A restoration algorithm that can use such a complex of data for 3-D image deconvolution is presented. It uses a Tikhonov-Miller regularization scheme and allows for the imposition of different types of constraints to obtain super-resolution deconvolved images. Performance was tested by using simulated 3-D imaging. An example is given of the restoration of a 3-D wide field optical image of a biological specimen in the presence of atomic force constraints.

Keywords: Image restoration, deconvolution algorithm, constraints, probe microscopy, NSOM, super-resolution.

1. INTRODUCTION

In the recent past there have been dramatic developments in optical microscopy. One stream of activity has been in far-field, wide field, optical imaging based on developments on the use of charge coupled devices or CCDs. It was recognized nearly 20 years ago by Agard and Sedat and their respective research groups[1,2] that the CCD is a powerful device that permits for digital imaging with very high stability, linearity and dynamic range. These workers also realised that such digital imaging was ideal for the revolution that was occurring in computational power and speed. This computer revolution led to a combination of experimental CCD imaging and image restoration. In effect the marriage between the CCD and computational image restoration has permitted three dimensional far-field optical imaging at resolutions that are comparable to confocal microscopy with the efficiency and light throughput of a wide-field microscope. [3] This paper takes this combination of CCD microscopy and image restoration and fully integrates it with the dramatic developments that have been occurring in scanned probe imaging. This marriage has the potential to enhance the expanding worlds of both far-field and scanned probe microscopy to achieve super-resolution imaging in three dimensions.

To appreciate this synergistic interplay of far-field and scanned probe imaging it is important to recall that the most successful algorithms that have been applied in fluorescence microscopy use prior knowledge regarding the object to be restored and the noise in the image. Examples of such algorithms are the constrained iterative algorithm of Agard *et al.,*[4] the regularized algorithm of Carrington,[3] the iterative constrained Tikhonov-Miller (ICTM) algorithm[5,6], the maximum *a posteriori* (MAP) [7,8] algorithm, and the expectation-maximization (EM)[9,10] algorithm. These algorithms possess super-resolution properties, allowing partial recovery of frequencies that are lost in the imaging process. In these algorithms a prior knowledge is used as deterministic constraints which reduce the set of feasible solutions and this is the basis for super-resolution. The more deterministic knowledge that is available the narrower is the set of feasible solutions and the better is the restored results.

The goal of this paper is to show experimentally and theoretically that the developments of near-field optical microscopy allow for a full integration of a scanned probe data set with a far-field digital image and this combination can provide powerful constraints for three dimensional deconvolution algorithms that have never been available before. In near-field optics a sub-wavelength point of light illuminates an object in the near-field before the light has a chance to loose its confinement as a result of diffraction[11]. The object is scanned pixel by pixel under this point of light and the amount of light either transmitted or reflected at each pixel is collected by a lens and detected by a point detector and placed in the memory of a desktop computer which forms the resulting image. Research in our laboratory has developed near-field

* Email: lewisu@vms.huji.ac.il

optical elements that are metal coated cantilevered optical fibers and these optical fibers are used for simultaneous near-field optical imaging and normal force atomic force microscopy topographic imaging of the object with nanometric resolution in x, y and z.[12-15]

Near-field optics has achieved the highest optical resolution that has ever been obtained. In addition, near-field optical approaches today give super-resolution topography to nanometer resolution in z and to at least 50 nm resolution in x and y. This has never been available in optics before. In near-field optics there is no Gaussian beam profile and no out of focus light so this is a method of spatial reduction in background in x, y and z. In spite of all these advantages near-field optics and the simultaneous atomic force microscopy imaging are not parallel imaging modalities as is the case in lens based microscopies and so they are slow. In addition, these scanned probe methods have little or no three dimensional imaging capabilities. The combination of scanned probe microscopic imaging with CCD digital microscopy and image restoration through the bridge that near-field optics provides has the potential to add the type of information to a far-field CCD data set that were simply impossible to obtain previously in far-field optical image restoration.

Experimentally the crucial requirement for this fusion of far-field and scanned probe data sets was the development of a near-field/atomic force microscope that could placed on any optical microscope without perturbing any of the myriad functions of the optical microscope. Such a development would allow for exact overlap of the scanned probe and CCD image through the optical tagging of the scanned probe coordinates with the near-field optical force sensor. In fact, developments in our laboratory have permitted such simultaneously imaging in a conventional optical microscope with an attached CCD and these developments form the basis of this paper. The results of such an integrated approach to microscopy allows for powerful deterministic constraints in image restoration algorithms for which there was a critical need but a paucity of such data.

2. THE EXPERIMENTAL SYSTEM

The experimental system that allows this fusion of data sets is shown in Figure 1. In this figure the near-field optical/atomic force microscope that is totally integrated into the optical microscope is shown diagrammatically placed on the sample stage of an inverted optical microscope above the lens of the microscope.

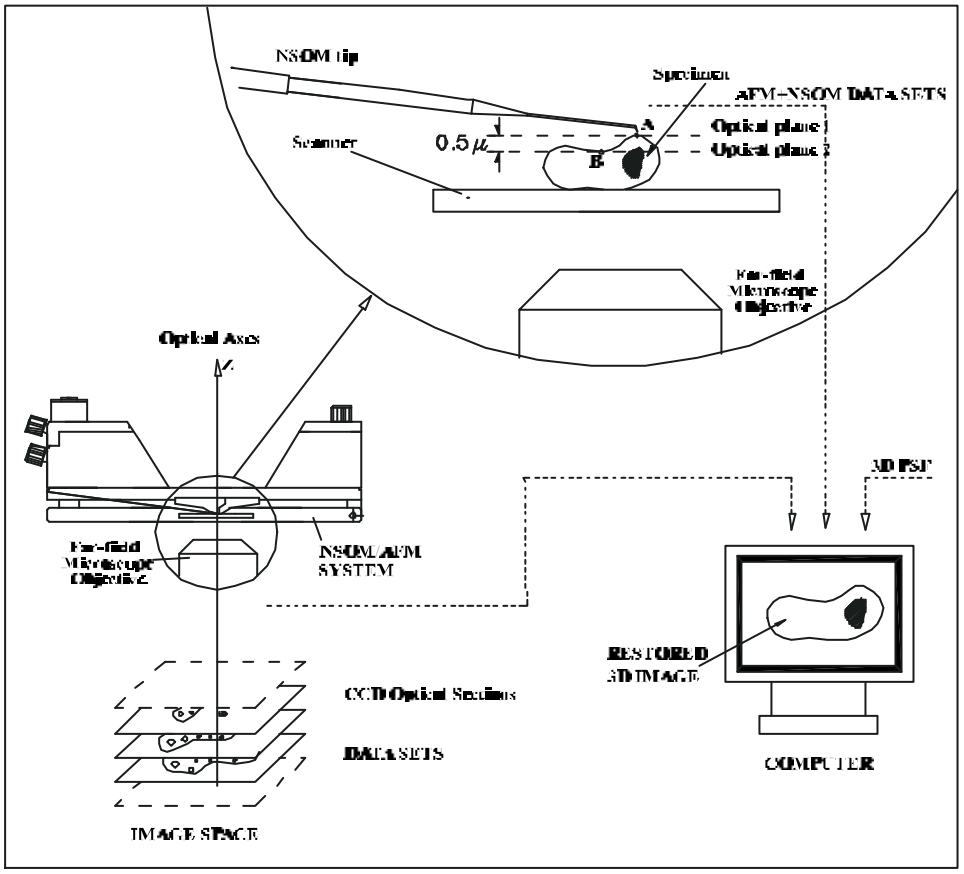

Fig.1 The Experimental Setup

The near-field optical tip is brought by normal force microscopy onto the object that is to be imaged with one of the modalities of atomic force microscopy. This includes either normal force contact mode, non-contact mode or intermittent contact. For the biological imaging done in this paper intermittent contact was used. The inverted microscope was fitted with a Princeton Instruments, Inc. imaging CCD cooled to liquid nitrogen temperatures to reduce the noise in the CCD. This CCD viewed the emitting cantilevered subwavelenght near-field optical and atomic force tip and allowed for a new dimension to be introduced in defining the local point spread function (PSF) of the lens with the perturbation of the sample fully accounted for and the position of the PSF fully defined. It also allows for powerful constraints such as a super-resolution tag of surface pixels and how they are related to the responding pixel of the CCD.

In terms of the PSF, the subwavelength dimension light source is an ideal point of light for determining the PSF. This is shown in Figure 2. In these images the in and out of focus point spread function over 4 microns with a z separation of 0.2 microns is displayed. As can been the full data set was readily obtained even with the sample in place with a very good signal to noise ratio. In the past where fluorescent beads have been used to measure such a PSF it was difficult to record the out-of-focus components of the PSF. Thus, this in itself allows for a significant improvement in even a conventional deconvolution without the imposition of the constraints that are a central feature of this paper.

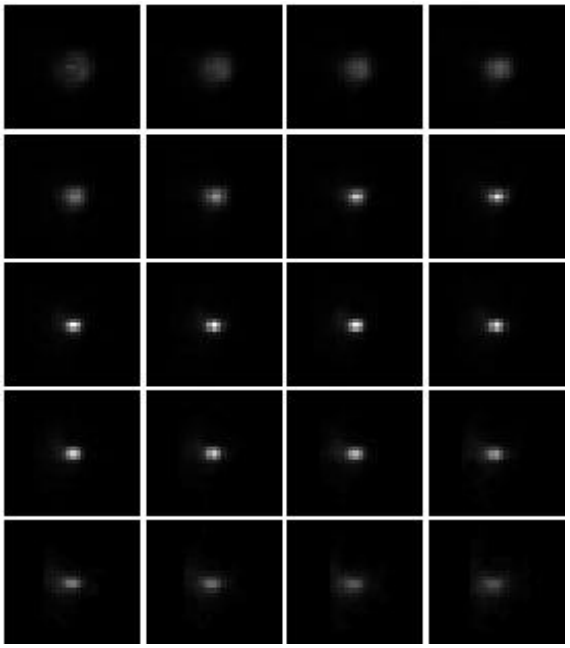

Fig. 2 CCD optical sections of the NSOM tip acting as a point source taken with a 63X 0.95 N.A. Ziess objective. The alteration in the z separation between each section is 0.2 microns. These sections are displayed with variable gain such that total intensity within each optical section has been normalized.

In terms of the super-resolution tagging of the surface pixels we see this in Figure 3. Figure 3A shows he in-focus point spread function of a subwavelength light source recorded by the CCD. The laser that was transmitted through the cantilvered tapered fiber tip was an all lines argon ion laser. In Figure 3B a CCD fluorescent image with mercury illumination is obtained while the tip is held in the same position with atomic force feedback. As can be seen in this frame the tip illumination is detected within the fluorescence of the surrounding sample. It is important to emphasize that both of these images were recorded without any movement of any component in the microscope. This permits the local detection of the PSF at any chosen location in the sample while the object that is being imaged remains in place.

In addition as noted above this approach also allows for tagging a particular position of the sample with the light that was emitted by the subwavelength point light source and to relate that position to a defined pixel of the CCD. This permits two points on the object surface that are separated in space by less than the far-field optical resolution to be defined with nanometric precision in terms of their spatial separation. This is shown diagrammatically in Figure 1 for height variations that are beyond the optical resolution. In this representation two optical planes at the surface of a specimen intersect the object at point A and B. Point A is shown being illuminated by the subwavelength point source that has a highly confined illumination volume in x, y and z. Thus the subwavelength point of light critically connects a location on an object of point A to a particular pixel of the CCD. A second point on the object, point B for instance in Figure 1, can be similarly tagged with the light emitting tip. Thus these two points can be differentiated in space even though they may not be resolved in the far-field optical imaging. The combination of AFM and the NSOM exactly identifies the spatial position of these two points with nanometric resolution. The excitation off fluorescent emission by this subwavelength point of light also has the potential to correlate surface variations in fluorescence intensity with spatial alterations between pixels.

The above shows that from the point of view of far-field optical microscopy the CCD acts as the digital bridge that connects the light of the near-field optical tip and the associated excited fluorescence intensity to the far-field image and from the point of atomic force microscopy the near-field optical tip acts as the optical bridge that can add light to a particular pixel of the CCD and allow for super-resolution correlation of this pixel with the other surface pixels using atomic force microscopy.

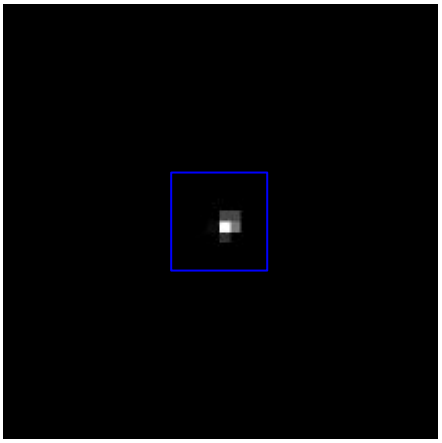

Fig. A CCD optical image of the NSOM tip which is in AFM contact with a fluorescent sample. The AFM contact is maintained by the AFM feedback system. Only light emitted by the tip is seen in this image.

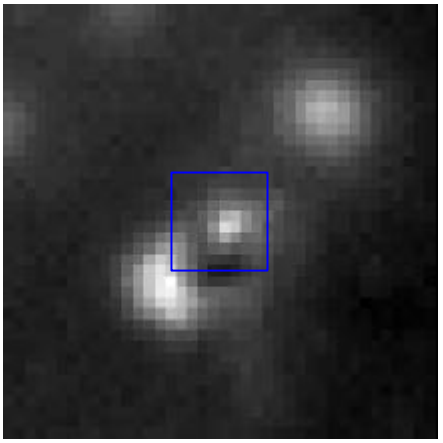

Fig. B CCD fluorescent image of the sample with the NSOM tip in AFM contact. The boxed region surrounds the pixels that include the response to the NSOM tip. The additional light that is detected by the surrounding pixels arises from the sample fluorescence.

3. DERIVATION OF THE ALGORITHM

The algorithm that has been developed to use these new constraints is a multiple constraint restoration algorithm based on Tikhonov-Miller regularization to solve the restoration problem. Simulated 3-D far-field images have been used to compare restoration results with and without support constraints, i.e. the constraints provided by the AFM delineation of the topography. We also present an example of the 3D restoration of the worm *C. elegans* imaged with an integrated wide-field optical/scanned probe microscope.

1. Imaging Model

We assume that we can model the imaging process by a following linear system of equations

$$g(x,y,z) = \sum_{i,j,k} h(x,y,z,i,j,k) f(i,j,k) + w(x,y,z) \qquad (1)$$

where $g(x,y,z)$ represents the 3D blurred noisy image, $f(i,j,k)$ represents the original 3D object as a matrix with a

size of $M \times N \times L$, $h(x,y,z,i,j,k)$ represents the blurring function, and $w(x,y,z)$ represents the noise process, for which we assume Gaussian zero-mean distribution with variance σ_w^2.

For this discussion a matrix notation is used and the image is converted into a vector by lexicographic ordering, leading to the image model

$$\boldsymbol{g} = \boldsymbol{H}\boldsymbol{f} + \boldsymbol{w} \tag{2}$$

where $\boldsymbol{f}$, $\boldsymbol{g}$ and $\boldsymbol{w}$ are the lexicographically ordered vectors of size $\times 1$ and $\boldsymbol{H}$ is the blurring matrix of size $\times$, where $= MNL$ is the dimension of the problem.

Solving $\boldsymbol{f}$ from (2) is an ill-conditioned problem, since $\boldsymbol{H}^{-1}$ may (in general) not exist. The pseudoinverse solution of Eq. (2) does exist but is unstable in the presence of noise. This problem has led to the application of a regularization procedure and prior knowledge to find a stable estimate of $\boldsymbol{f}$.

2. Multiple Constraints Restoration Approach Based on Tikhonov-Miller Regularization

Consider the estimate $\hat{\boldsymbol{f}} \in$ of the inverse restoration problem (2) which satisfies constraint conditions provided by a *priori* knowledge about the object. Each constraint condition defines a subset $\boldsymbol{W}_i$ that is a subspace of the total space $\boldsymbol{W}_i \subset$. The set of feasible solutions $\boldsymbol{W} \subset$ is then the intersection of all constraint sets $\boldsymbol{W}_i$.

$$\boldsymbol{W} = \bigcap \boldsymbol{W}_i \tag{3}$$

The set of feasible solutions is primarily populated with unacceptable solutions because of the ill-conditioned nature of the restoration problem. Its stabilization can be achieved by minimization of some stabilizing functional $(\boldsymbol{u})$ on the set of feasible solutions $\boldsymbol{W}$. This is known as Tikhonov regularization. Thus, the stabilized estimate $\hat{\boldsymbol{f}}$ of the inverse restoration problem (2) is the minimum of $(\boldsymbol{u})$ on $\boldsymbol{W}$.

$$\min_{\boldsymbol{u}} \{ (\boldsymbol{u}) \quad \text{such that} \quad \boldsymbol{u} \in \boldsymbol{W} \} \tag{4}$$

A wide class of different stabilizing functionals was described in the literature, including for example, the bounded variation[6], maximum entropy[8] and Good roughness[8] measures.

Let us now suggest several examples of constrained sets that can effectively deal with the type of constraints that this integrated method of microscopy can provide.

1) *Bounded norm residual*

On the basis of equation (2) we can define a set of bounded norm residuals as the following

$$\boldsymbol{W}_1 = \{ \in \; | \quad \| \boldsymbol{g} - \boldsymbol{H}\boldsymbol{u} \| \le \boldsymbol{e} \} \tag{5a}$$

where $\boldsymbol{e} = \|\boldsymbol{w}\| = \sqrt{} \boldsymbol{s}_{\boldsymbol{w}}^2$ is the noise level.

Generally the noise level $\boldsymbol{e}$ can be estimated from the region of the image in which there is no object. This type of constraint can be applied to all restorations including those that only include far-field optical data sets.

2) *Object support constraint*

This constraint considers the use of the AFM data as it relates the object topography to the optical CCD data. Thus we can determine which pixels in the image space correspond to the exact boundary of the object. These pixels define the object support in the image space . Therefore, on domain which is the complement of in the value of the restored image should be zero.

We thus define the object support constraint set $\boldsymbol{W}_2$ as the following

$$\Omega_2 = \{u \in \mathbb{R}^N \mid u_j = 0 \quad \text{for} \quad j \in \bar{\Omega}\} \tag{5b}$$

3) *Nonnegative constraint*

The intensity distribution of the fluorescence through the object is a nonnegative function. This defines the natural physical constraint on a restored image. The nonnegative constraint set is the following

$$\Omega_3 = \{u \in \mathbb{R}^N \mid u_j \geq 0 \quad \text{for} \quad j \in \Omega\} \tag{5c}$$

The above constraints allow for effectively defining the set of feasible solutions.

Given $\Omega = \Omega_1 \cap \Omega_2 \cap \Omega_3$ the constraint minimization problem (4) for the stabilized estimate $\hat{f}$ can be formulated in the equivalent form

$$\min_u \{\|g - Hu\|^2 + \alpha \cdot \Phi(u) \quad \text{such that} \quad u_j = 0 \text{ for } j \in \bar{\Omega} \quad \text{and} \quad u_j \geq 0 \text{ for } j \in \Omega\} \tag{6}$$

where α is the regularization parameter which is chosen so that condition $\hat{f} \in \Omega_1$ is satisfied. The minimization problem (6) is easy for practical implementation since it has a simple linear equality and inequality constraints.

3. The Multiple Constraints Restoration Algorithm

We have developed an algorithm for solving the constraint minimization problem as described in Equation 6. This algorithm was built around a commercially available software package Matlab (Math Works Inc.) that provides a large-scale optimization routine. This routine is based on the interior-reflective Newton method described in.[16] Each iteration involves the approximate solution of a large linear system using the method of preconditioned conjugate gradients (PCG). Such an algorithm converges very rapidly to an optimal solution.

4. THEORETICAL SIMULATION OF THE APPROACH

To investigate the properties of the multiple constraints algorithm above, we performed simulations, representative of imaging in a wide field optical microscope. We have created a synthetic object consisting of a hollow ellipsoid and embedded in it is a smaller solid sphere. The object was generated on a $64 \times 64 \times 64$ sampling lattice. The intensity of the ellipsoid shell was normalized to one, the intensity of the inner part of the ellipsoid was 0.2 and the intensity of the small sphere was 0.6. The simulated wide field optical image was obtained by convolving the object with an experimental 3D PSF. A white Gaussian noise of level 0.01 was added. Figures 4 shows the XY and XZ image sections of the object and of the blurred image.

The 3D image restoration was performed by using the multiple constraints restoration algorithm described above. From a mathematical point of view, this algorithm solves the constraint minimization problem (4). In the particular case where an object support constraint is given, this problem is reduced to the constraint minimization problem (6). To simulate the constrained set of the AFM data we have assumed that we know exactly where the border of the object is situated in the image space. Thus the set $\bar{\Omega}$ in the constraint minimization problem (6) consists of all pixels which are outside the spatial domain of the object. For solving this problem a stabilizing functional $\Phi(u)$ needs to be chosen. We have chosen the stabilizing functional of the form

$$\Phi(u) = \|Lu\|^2 \tag{7}$$

where the matrix L represents 3D Laplacian operator. For a choice of the regularization parameter α in (6), which is critical for a good restoration result (since it determines the trade-off between fitting and smoothing the solution) we have empirically chosen for this simulation example the value of $\alpha = 0.002$. The result of the constrained restoration with this algorithm is shown in Figure 5A (left image) and in Figure 5B (left image). In Figure 5A (right image) and in Figure 5B (rigth image) is shown the restoration result without the imposition of the support constraint.

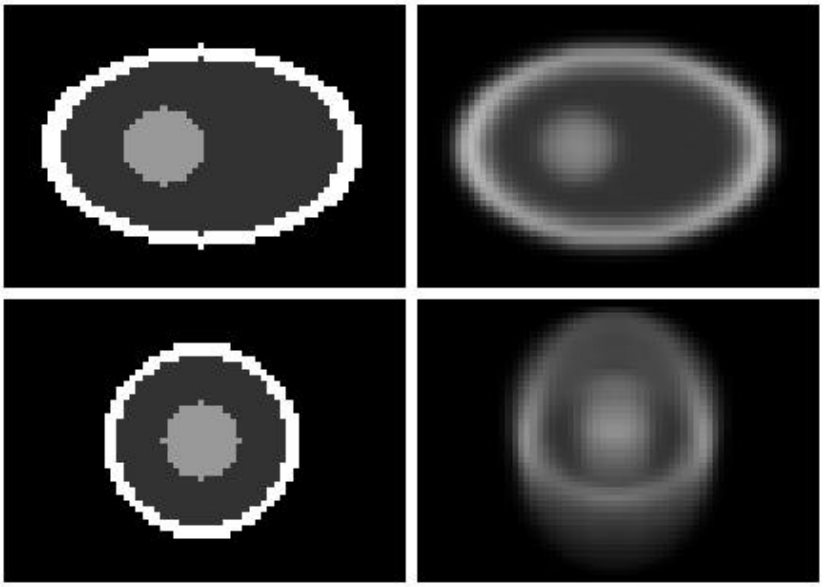

Fig 4 The top left and the top right images are the XY sections of the model object and of the blurred image respectively. The bottom left and the bottom right images are the XZ sections of the model object and of the blurred image respectively.

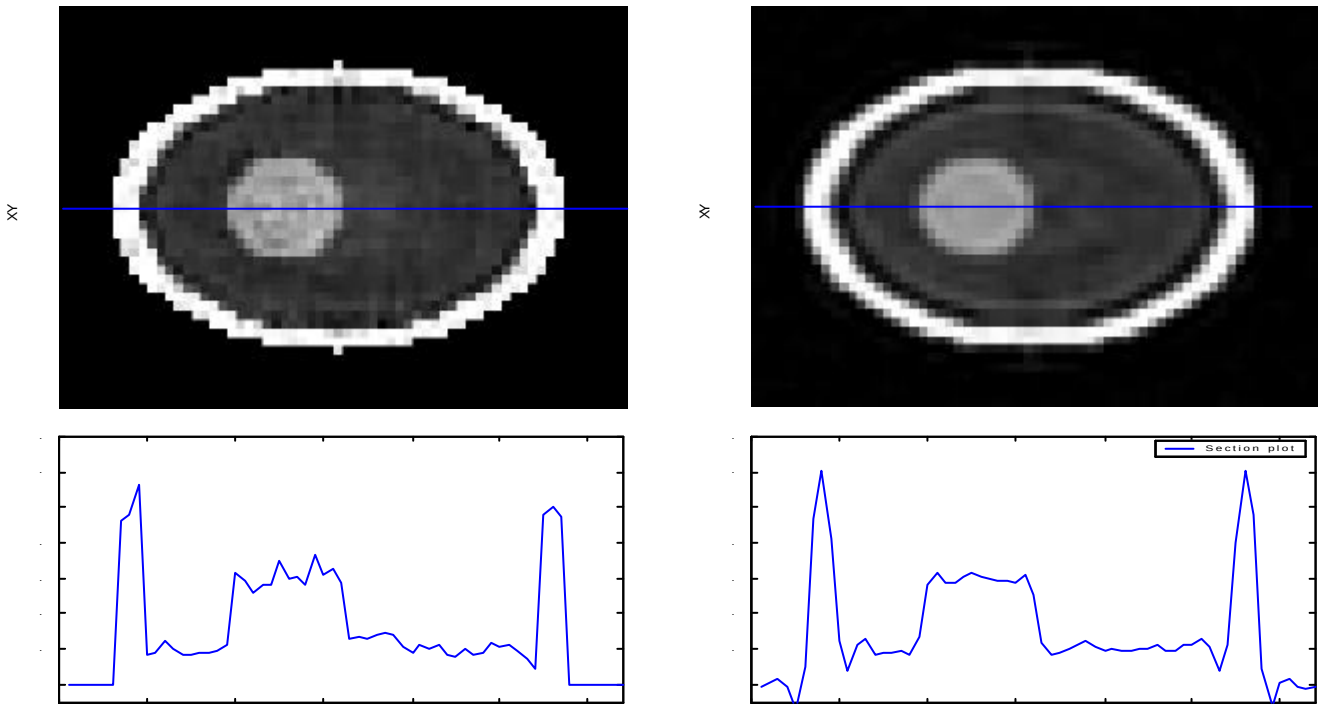

Fig. 5A. Left column corresponds to XY sections of the 3D restored image with the application of the support constraint condition. Right column corresponds to XY sections of the 3D restored image without application of the support constraint conditions.

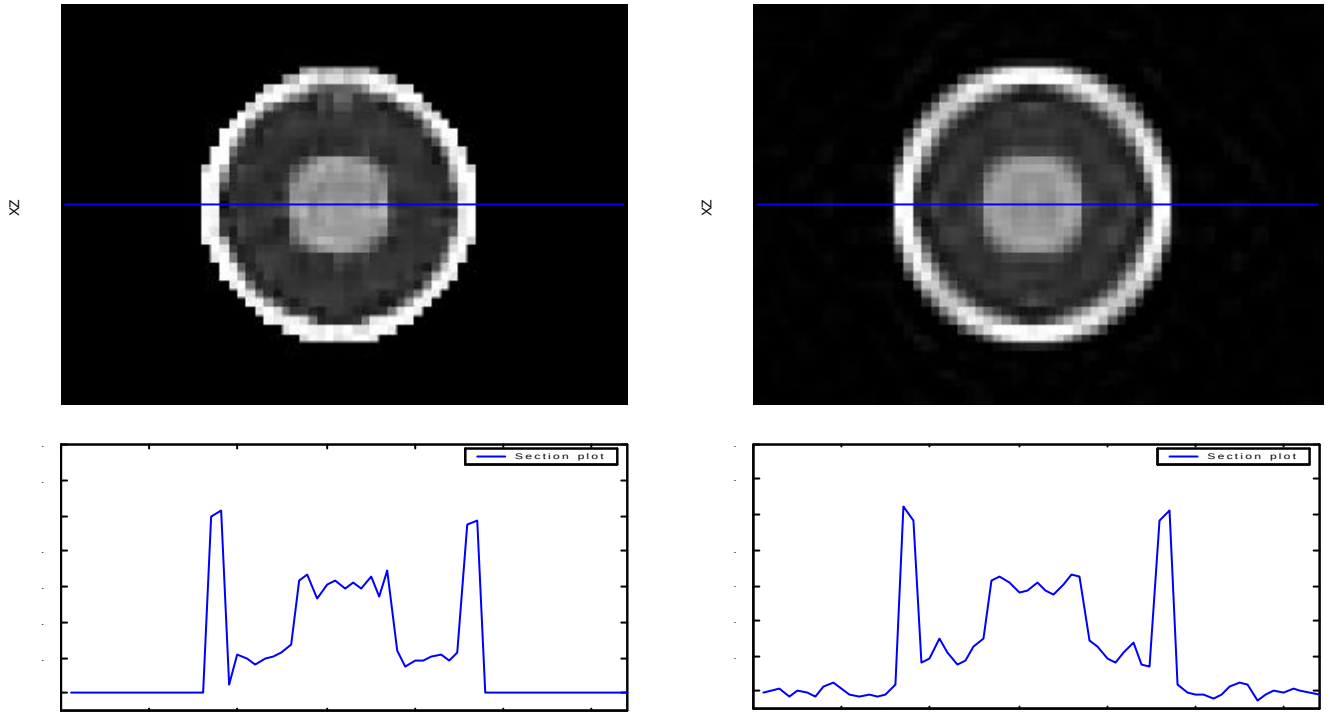

Fig. 5B Left column corresponds to XZ sections of the 3D restored image with the application of the support constraint condition. Right column corresponds to XZ sections of the 3D restored image without application of the support constraint conditions.

The analysis of the restored images shows that the constraint method leads to a better restoration than the unconstrained method. In particular, the shape of the synthetic object is restored very well. This is not surprising, since the outer borders of the object were predefined by the constraint condition. In addition to this, the constrained restored image has less artifacts than the unconstrained image. For example notice that in the unconstrained deconvolution dark artifactual rings appear in the inside of the border (Figures 5A right image). In addition, in the right image of Figure 5B light is seen outside the border of the object. Furthermore, in the constrained deconvolution notice that these artifacts are not observed and that the central object is better reproduced.

5. EXPERIMENTAL APPLICATION OF THE APPROACH AND ALGORITHM

To test this integrated approach to microscopy and the associated algorithm for image restoration we have investigated the possibility of applying this fusion of imaging modalities to a complex biological object. We show that this new approach results in significant improvements in the 3D deconvolution relative to the use of state of the art image restoration routines that do not use the constraints that we can now provide.

1. Application to a Complex Biological Imaging Problem

For investigating the ability of applying this approach to microscopy to a complex biological imaging task we have applied our approach to the non-parasitic, soil dwelling, nematode *C. elegans.* Green fluorescent protein (GFP) from the jellyfish *Aequorea victoria* can be genetically expressed in *C. elegans* and can be used for monitoring the localization of specific proteins and even the membrane potential at specific sites in specific cells[17]. For our measurements we used a transgenic animal with an integrated DES-2-GFP (S65C) chimera (DES-2 is a subunit of the DES-2/DEG-3 nicotinic acetylcholine receptor (nAChR). Thus, wherever this receptor was expressed in this transgenic animal a fluorescent GFP was also present.

In Figure 6 the CCD image of *C. elegans* is seen with an illuminating subwavelength cantilevered optical fiber tip in place. In this Figure the point on the *C. elegans* that is tagged with this point of light correlates this point to the pixel of the CCD that is responding. The square box that is shown in the figure indicates the extent of the AFM scan.

The corresponding AFM image of the *C. elegans* Figure 7 accurately indicates the border of the animal in this region with nanometric precision. Such data has been used as one of the constraints in the image restoration that is described above.

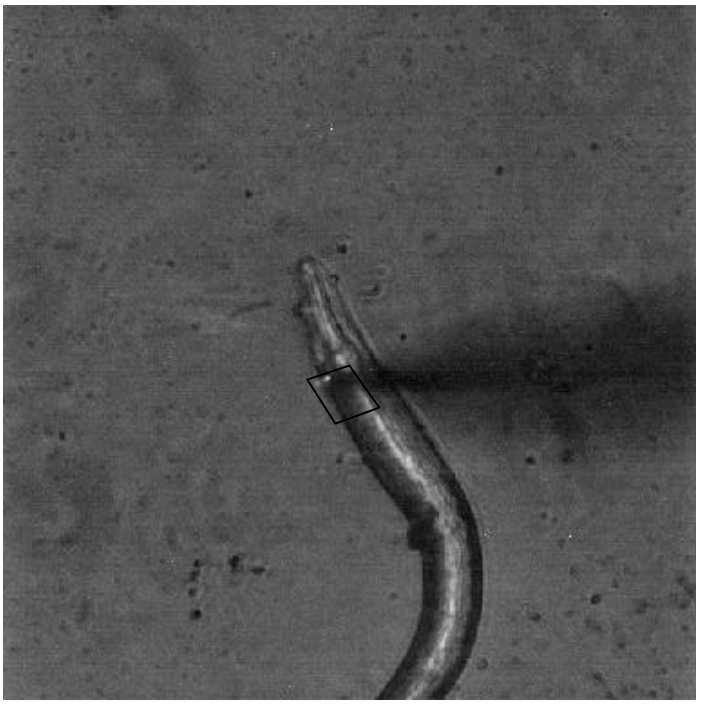

Fig. 6 The CCD optical image of *C. elegans* with an illuminating subwavelength cantilevered optical fiber tip. The square box indicates the extent of the AFM scan.

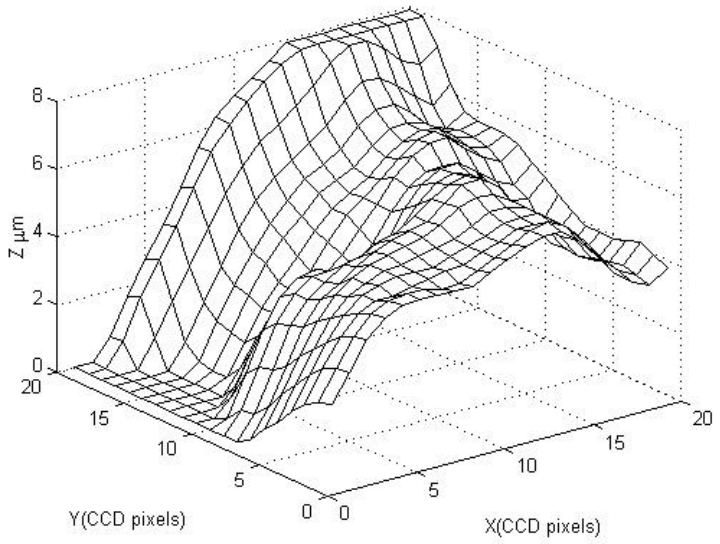

Fig. 7 The AFM data corresponding to the box region in Figure 6.

In Figure 8A optical sections through a GFP labeled *C. elegans* is obtained. As can be seen with this magnification and numerical aperture there is very little discrimination between the various optical sections. This can be improved by using the algorithm described in section 3 without the imposition of constraints (see Figure 8B). The results of introducing only the AFM data as a constraint is shown in Figure 8C. As can be seen, with constraints the restoration produces significant alterations in similar optical sections. For example, in the (1,1) and (1,2) sections of Figure 8C (where n,m corresponds to the n row and m column) there is a significant reduction in the illuminated pixels. Look at the border of the worm which has been very effectively defined by the AFM constraint that has been applied. In addition, there are even optical sections such as (2,2) and (2,3) in which the unconstrained algorithm shows fluorescence and the constrained algorithm does not report any fluorescence.

This initial application of such an integrated approach to scanned probe and optical data sets indicates that there is significant potential in the approach. The next step will be to insert the surface fluorescence of the biological object using near-field optics and to use this data set as an additional constraint in the multiple constraints algorithm described above

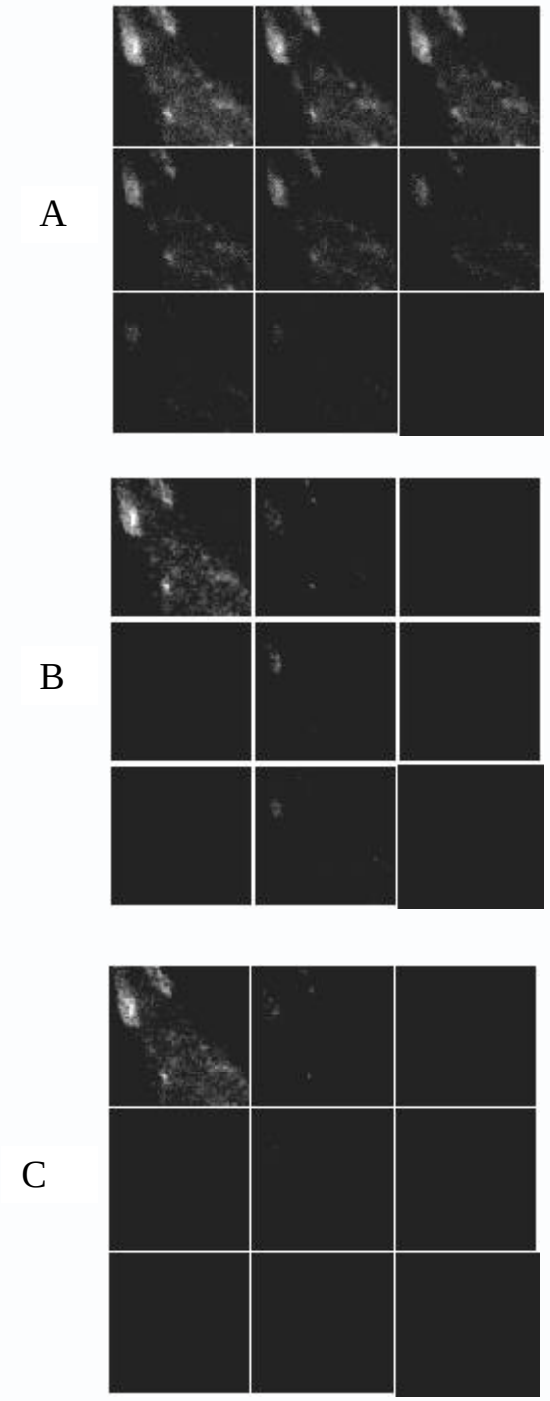

Figure 8. A. Optical sections through the worm *C. elegans* that is genetically expressing the green fluorescent protein (GFP) with the nicotinic acetylcholine receptor (nAChR), DES-2/DEG-3. B. An unconstrained 3D deconvolution of the data set shown in A. C. A 3D deconvolution of the data set shown in A using the AFM data as a constraint and the constrained deconvolution algorithm that has been developed.

ACKNOWLEDGMENTS

The authors would like to acknowledge the Israel Ministry of Science Scientific Infrastructure Program in Microelectronics for support of this work. The authors would also like to thank Dr. Uzi Efron, the scientific advisor of the above program for his strong support of this research effort. Mr. Anatoly Komissar of Nanonics Imaging Ltd is also thanked for technical help in many aspects of this project.

REFERENCES

1. -dimensional a , *Nature* **302**, pp. 676-681, 1983.
2. Fluorescence microscopy in three dimensions, *Methods Cell Biol*. **30**, 353-377, 1989.
3. W. A. Carrington, R.M. Lynch, E.D.W. Moore, G. Isenberg - *Science* **268**, pp. 1483-1487, 1995.
4. *Annu. Rev. Biophys. Bioeng.* **13**, pp. 353-377, 1984.
5. A. N. Tikhonov, and V. Y. Arsenin, *Solutions of Ill-Posed Problems*, Wiley, New York, 1977.
6. Analysis of bounded variation penalty methods for ill-posed problems blems, **10**,1217-1229,1994.
7. a posteriori *J. Opt. Soc. Am. A.* **14,** pp 1696-1706, 1997.
8. P.J Verveer, M. - dimensional confocal and wide- *J. Microsc.*, **193**, pp. 50-61, 1999.
9. *J. R. Stat. Soc. B* **39**, 1-38, 1977
10. R. L. Lagendijk, and J. Biemond, *Iterative Identification and Restoration of Images*, ch.7-8, Kluwer Academic,1991
11. A. Lewis, M. Isaacson, A. Spatial Resolution Light Microscope: Light is Efficiently Transmitted through λ **13**, 227-232, 1984.
12. S. Shalom, K. Lieberman, A. Lewis and S. R. Cohen, "A Micropipette Force Probe Suitable for Near-field Scanning Optical Microscopy," *Rev. Sci. Instr.* **63**, 4061, 1992
13. K. Lieberman, A. Lewis, G. Fish, T. Jovin, A. Schaper and S. R. Cohen, "Multifunctional, Micropipette Based Force Cantilevers for Scanned Probe Microscopy," *Appl. Phys. Lett.* **65**, 648-650, 1994.
14. A. Lewis, K. Lieberman, N. Ben-Ami, G. Fish, E. Khachatryan, U. Ben- New Design and Imaging Concepts in NSOM *Ultramicroscopy* **61**, 215-220, 1995.
15. Fujihira, APL 1995, K. Lieberman, N. Ben-Ami and A. Lewis, "A Fully Integrated Near-field Optical, Far-field Optical, Confocal and Normal-Force Scanned Probe Microscope," *Rev. Sci. Instr.* **67**, 3567, 1996.
16. A Reflective Newton Method for Minimizing a Quadratic Function Subject to Bounds on of the Variable, *SIAM Journal on Optimization* **6**, pp. 1040-1058, 1996.
17. A. Lewis, A. Khatchatouriants, M. Treinin, Z. Chen, G. Peleg, N. Friedman, O. Bouevitch, Z. Rothman, L. Loew and teins and Imaging Membrane Potential Around GFP Molecules at Specific Sites in Neuronal Cells of *C. elegans Chem. Phys.* **245**, pp. 133-144, 1999.